Journal of The Electrochemical Society, **161** (9) A1247-A1252 (2014)
0013-4651/2014/161(9)/A1247/6/$31.00 © The Electrochemical Society

Numerical Study of Interaction and Aggregation of Non-Spherical Particles in Forming Li-Ion Battery Cathodes

Min Zhu,[a] Jonghyun Park,[a] A. M. Sastry,[b] and Wei Lu[a,z]

[a]*Department of Mechanical Engineering, University of Michigan, Ann Arbor, Michigan 48109, USA*
[b]*Sakti3, Ann Arbor, Michigan 48108, USA*

Aggregation between additive particles and active particles in battery electrode material strongly affects their interfacial phenomena and eventually battery performance. This paper proposes a three dimensional model to simulate the aggregation process of spherical carbon black (CB) and ellipsoidal $LiMn_2O_4$ active material (AM) particles within a liquid medium (PVDF polymer dissolved in NMP solvent) in the electrode materials of Li-ion batteries. Monte Carlo method is employed and the resulting aggregates are characterized by the number of CB particles connected to the percolated cluster of AM, which affects the effective conductivity. The effects of particle geometry and constituent mass ratio are investigated. It is found that a larger AM particle aspect ratio contributes positively to the percentage of CB attachment. For a given AM particle aspect ratio of 2 or 3, the average percentage of CB attachment is found to decrease as the CB:AM mass ratio increases from 2%:94% to 4%:92%.
 [DOI: 10.1149/2.0211409jes]

Manuscript received March 12, 2014. Published June 3, 2014.

Li-ion batteries have become the primary choice of power source for modern electric vehicles (EV) and hybrid electric vehicles (HEV) as the cost per watt-hour has continued to decrease in recent years. However, the low conductivity of active materials (AM) limits battery power performance, which is one of the major challenges of Li-ion batteries used in EV and HEV applications. Although the conductivity of electrodes can be improved by adding conductive additives [e.g. carbon black (CB)], the total mass of the battery is increased due to these inactive additives, thus lowing gravimetric energy and power density. The CBs are also related to the electrolyte oxidation reactions,[1,2] active material dissolution,[1–4] and impediments to Li-ion intercalation,[5,6] all of which may degrade battery performance.

Several experimental studies have shown that different self-assembled characteristic structures are formed from active material particles, conductive additive particles and polymer binder materials [e.g. polyvinylidene difluoride (PVDF), polytetrafluoroethylene (PTFE)]. The morphology of these characteristic structures varies according to the composition of the electrode materials. The morphology determines whether or not conductive additive can effectively form a conductive network, and it also plays an important role in the structural integrity of the particle network. Therefore, it would be beneficial if one could control the self-assembly process of these electrode constituents to improve capacity and power density while keeping parasitic mass to a minimum.

In our previous efforts to optimize the composition of the cathode, Brownian dynamics simulations with binary spherical particle system have been conducted, and the effects of several key parameters have been identified.[7] However, the geometries of real particles in Li-ion battery electrodes generally depart from purely spherical;[8–10] this departure changes surface area,[11,12] reaction rate,[13] stress distribution due to Li intercalation,[14] and other electrode properties. In order to study more general cases of electrode particles and provide more powerful tools to analyze the mechanics of realistic electrode particles, it is necessary to model the interaction between non-spherical particles.

A major challenge of including non-spherical particles is evaluating the interaction energy among the particles. In cases where the pair-wise additive inverse power law potential (such as van der Waals energy) is considered, the potential of particle-particle interaction can be obtained by integrating over the volumes of the interacting bodies.[15] However, explicit expressions are only available for simple geometries. The explicit expression of the interaction energy for ellipsoidal particles has not been formulated. Efforts have been made to obtain the value of the interaction energy using methods that are less computationally intensive than numerical integration over ellipsoid volumes. Empirical potential functions have been proposed for ellipsoids with certain types of interaction potential profiles.[16] When considering the interaction based on the pair-wise additive potential, a boundary element method was also proposed,[17] which converts a volume expression into surface integrals that are then calculated by discretizing the surface of the object into triangular elements.

A perturbative expansion in the dielectric contrast which converges rapidly for particles at small separations has been proposed.[18] The Derjaguin approximation has been applied in the colloidal aggregation simulation,[19–21] greatly simplifying the calculation of interaction forces under the assumption that with a short distance between particle interfaces a relatively small region contributes almost all the interaction energy between the interacting convex particles. However, the approximation is only valid for an interaction distance several times smaller than the particle size. For long separation distances, the interaction energy quickly approaches zero; however, for intermediate ranges where the separation distance is comparable to the size of the interacting particles, the above-mentioned approximation diverges from the exact value, thus rendering the approximation unsuitable for the electrode particle aggregation process that we are interested in.

A method that is both capable of accurately finding the interaction potential between generally shaped particles such as ellipsoids, and at the same time computationally efficient enough to be used during aggregation simulation, is not available from the literature; this is due to the high computational cost associated with the numerical integration and the limitations of the applicable ranges of the approximation method. Therefore, the objectives in this work are as follows:

1) develop a fast approach to finding the interaction energy among non-spherical particles and to modeling the self-assembly process for the constituent materials of an electrode during its fabrication
2) characterize the self-assembled structures and identify the effect of particle geometry

Methods

Monte Carlo simulation.— We performed Monte Carlo simulations to model the aggregation of CB and AM particles. The followings include the details about 1) how to initialize the system for a specific packing density and 2) how to move particles in the Monte Carlo simulation and detect overlapping between particles. Periodic boundary conditions were applied to the simulation cell.

Initial configuration.—In order to achieve the desired packing density, we employed a concurrent construction method to generate the initial configuration of ellipsoidal particles.[22–24] The process is similar to conventional molecular dynamics except for a few major differences. The concurrent construction process starts with a collection of randomly dispersed points of infinitesimal size. The particles enlarge uniformly and evenly in each time step until they become ellipsoids with a long semi-axis, $a(t)$, and two short semi-axes, $b(t) = c(t)$. The

[z]E-mail: weilu@umich.edu

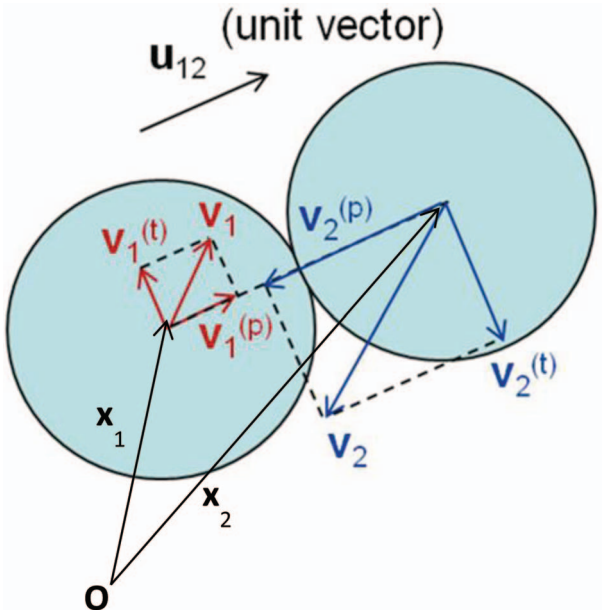

Figure 1. Velocity components for two particles (simplified as spheres).

initial translational and rotational velocities of the infinitesimal particles are assigned randomly, and the particles are allowed to elastically collide with each other at each time step as they enlarge. When particles collide, momentum transfer occurs. The purpose of this particle growth stage is not to simulate a physical process, but to generate a relatively densely packed initial configuration (without penetration) for the main simulations. Thus, several simplifications are made in the collision algorithm to reduce computational cost at this stage. We simplify the linear momentum transfer between ellipsoids using the model of spheres of equal volume.[22] The translational velocities of two particles of the same size (number 1 and 2) are denoted $\mathbf{V}_1$ and $\mathbf{V}_2$, just before the collision. These two velocities are resolved into parallel (p) and transverse (t) components with respect to the line of particle centers as shown in Fig. 1:

$$\mathbf{V}_1 = \mathbf{V}_1^{(p)} + \mathbf{V}_1^{(t)} \quad [1]$$

$$\mathbf{V}_2 = \mathbf{V}_2^{(p)} + \mathbf{V}_2^{(t)} \quad [2]$$

The equations of the momentum transfer between particles of equal size (growth rate are set to be the same for all ellipsoids) are given by

$$\mathbf{V}_1^* = [\mathbf{V}_2^{(p)} + h\mathbf{u}_{21}] + \mathbf{V}_1^{(t)} \quad [3]$$

$$\mathbf{V}_2^* = [\mathbf{V}_1^{(p)} + h\mathbf{u}_{12}] + \mathbf{V}_2^{(t)} \quad [4]$$

where $\mathbf{V_1}^*$ and $\mathbf{V_2}^*$ denote the velocities just after impact. The transverse velocity components remain unchanged after impact, whereas the parallel components are swapped and modified in magnitude by adding a growth term $h\mathbf{u}_{12}$ to account for the increase in linear momentum due to mass increase.[22] Here $\mathbf{u}_{12}$ is the unit vector pointing from the center of particle 1 to the center of particle 2,

$$\mathbf{u}_{12} = \frac{\mathbf{x}_2 - \mathbf{x}_1}{|\mathbf{x}_2 - \mathbf{x}_1|} = -\mathbf{u}_{21} \quad [5]$$

where $\mathbf{x}$ is the position vector of the particle center. The parameter h is defined as the growth rate of the long semi-axis of the particle,

$$h = \frac{da(t)}{dt} \quad [6]$$

The long semi-axis is used in the above equation to make sure that the two particles will always move apart by a distance longer than the increase in particle size at each time step. Therefore, particles will not end up in an overlapping position after collision. As for the rotational velocities of the two ellipsoidal particles, a physically realistic collision model will require the determination of contact points at the surface of each ellipsoid in order to determine the changes in rotational velocity based on the rigid body motion. For the purpose of this work, a simplification is made and random rotational velocities are assigned to the two particles after collision. If the new rotational velocities result in particle overlapping at the next simulation time step, they are rejected and a new value is assigned until no overlapping occurs at the next time step.

Monte Carlo movement.—After the ellipsoidal active material particles are generated, they are subject to Monte Carlo simulations until a stable configuration is achieved. Next, the smaller carbon black particles are randomly placed in the simulation cell, and subsequently both the active material particles and the carbon black particles are subjected to Monte Carlo movements until a stable configuration is reached. When the center-to-center distance between two particles are less than the threshold distance (1.01 r_0 for AM-AM and AM-CB interaction, 1.001 r_0 for CB-CB interaction, where r_0 is the center-to-center distance when two particles touch each other.), the two are considered to belong to the same cluster. With each move, a single particle or a single cluster is randomly selected and displaced. For a particle, the magnitude and direction of the translational displacement is randomly assigned based on the Gaussian distribution. For an ellipsoidal particle, another vector is added to the unit vector representing the orientation of the axis of revolution. The magnitude and direction of the added vector is also randomly assigned based on the Gaussian distribution. The new orientation vector is then normalized. If a cluster is selected, it is treated as a rigid body, and the configuration of its particles remains unchanged. The center of one of the particles within this cluster is randomly picked to be used as the rotational center of the rigid motion of the entire cluster. The translational and rotational vectors are assigned randomly following the Gaussian distribution. If the moved particle(s) overlaps with any other particle, the move is rejected and the algorithm repeats the previous procedures by selecting a new particle and performing a trial move. If no overlapping is detected, the change in energy for the entire system is calculated, and the Monte Carlo move is accepted based on the probability as follows,

$$\mathrm{P\,(accept)} = \begin{cases} \exp\left(-\dfrac{E_{new} - E_{old}}{k_B T}\right); & if \quad E_{new} > E_{old} \\ 1; & if \quad E_{new} \le E_{old} \end{cases} \quad [7]$$

where P(accept) is the probability that the Monte Carlo move will be accepted, E_{new} is the energy of the new configuration after the Monte Carlo move, E_{old} is the energy of the old configuration, k_B is the Boltzmann constant, and T is the absolute temperature.

Overlapping detection.—Throughout the Monte Carlo simulations, an overlapping detection algorithm is used to check whether two ellipsoids overlap with each other, and the movement is rejected if overlapping occurs. The algorithm was developed for ellipsoids of revolution with equal size,[25,26] which is suitable for the system in this work. The necessary and sufficient condition for two ellipsoids to have no real point in common or to be exteriorly tangent is that the functions ψ, S_1 and S_2 be positive or zero, and at least one among g_1, g_2 and m be negative.

$$g_\alpha = 4 + \left(\frac{a}{b} - \frac{b}{a}\right)^2 (\mathbf{u}_1 \times \mathbf{u}_2)^2 - \frac{|\mathbf{d}|^2}{b^2} + \left(\frac{1}{b^2} - \frac{1}{a^2}\right)(\mathbf{d} \cdot \mathbf{u}_\alpha)^2 \quad (\alpha = 1, 2) \quad [8]$$

$$m = g_1 + g_2 - 2 - \frac{1}{b^2}\left(\frac{a}{b} - \frac{b}{a}\right)^2 [(\mathbf{u}_1 \times \mathbf{u}_2) \cdot \mathbf{d}]^2 \quad [9]$$

$$p = -m \quad [10]$$

$$q = g_1 g_2 - 4 \quad [11]$$

$$w = 4m - g_1^2 - g_2^2 \quad [12]$$

$$\psi = 4(p^2 - 3q)(q^2 - 3wp) - (9w - pq)^2 \quad [13]$$

$$S_1 = m^2 - 2g_1 g_2 - 4 \quad [14]$$

$$S_2 = g_1^2 g_2^2 + 8g_1 g_2 - 2m\left(g_1^2 + g_2^2\right) \quad [15]$$

where $\mathbf{u}_1$ and $\mathbf{u}_2$ are the unit vectors of the axes of revolution for the two ellipsoids (a is along the axis of revolution) and $\mathbf{d}$ is the vector connecting the center points of the two ellipsoids.

Interaction energy look-up table.— We employed the Hamaker theory to find the interaction potential between two arbitrarily-shaped particles.[15] Ignoring multibody interactions, we consider the interactions to be pair-wise. The Gibbs free energy due to the dispersion interaction can be expressed as

$$\Delta G_{12}^d = -\int_{V_1} dV_1 \int_{V_2} \frac{\Lambda_{12}\rho_1\rho_2}{r_{12}^6} dV_2 \quad [16]$$

where Λ_{12} is the London coefficient for two molecules, V_1 and V_2 are the volumes of two particles, r_{12} is the distance from one point in particle 1 to one point in particle 2, and ρ_1 and ρ_2 are the molecular number densities (number of molecules per unit volume). In the special case of two interacting spheres with an equal radius of a_0 and a distance of d between the centers, the free energy can be expressed as

$$\Delta G_{12}^d = -\frac{A_{12}}{6}\left[\frac{2a_0^2}{d^2 - 4a_0^2} + \frac{2a_0^2}{d^2} + \ln\left(1 - \frac{4a_0^2}{d^2}\right)\right] \quad [17]$$

where A_{12} is the Hamaker constant

$$A_{12} = \pi^2 \rho_1 \rho_1 \Lambda_{12} \quad [18]$$

However, for the interaction between the two ellipsoids of which the semi-axes are of different lengths, no algebraic form is available for the ΔG_{12}^d in Eq. 16. Numerical integration methods can be employed to calculate the interaction potential, but they are too computationally expensive to be incorporated in each time step of the Monte Carlo simulation. To accelerate the process of finding the interaction potential, we developed a look-up table. We first parameterized the relative position and orientation of two particles and calculated the interaction potential over the entire range of these parameters. The interaction potential between two particles can then be obtained by interpolation using the look-up table.

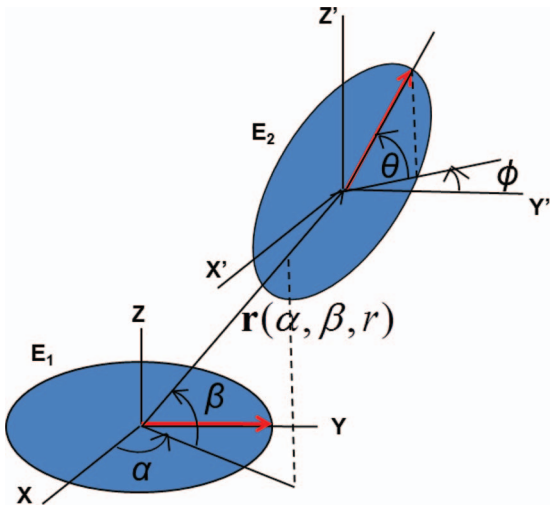

Figure 2. Relative position and orientation between two equal ellipsoids of revolution.

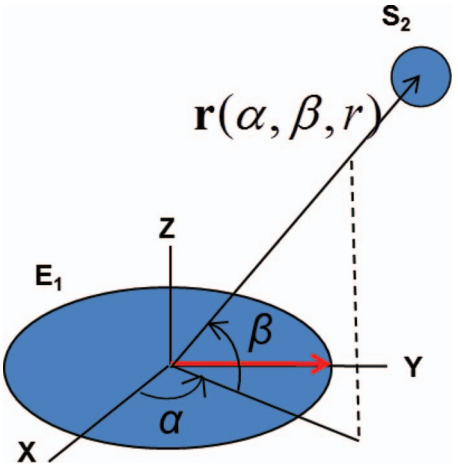

Figure 3. Relative position and orientation between one ellipsoid (E_1) and one sphere (S_2).

In this work, active material particles are modeled as prolate spheroids, and carbon black particles are modeled as spheres. As shown in Fig. 2, for any two given ellipsoidal particles E_1 and E_2, a Cartesian coordinate system (X-Y-Z) is chosen so that the Y-axis is in line with the axis of revolution of E_1, and the origin of the coordinate system is located at the center of E_1. The center of ellipsoid E_2 is expressed with the polar angles α, β, and the distance r with respect to the coordinate system X-Y-Z. The directional vector of the axis of revolution of ellipsoid E_2 can be expressed by the Euler angles φ and θ. Therefore, five parameters are required to describe the relative position between the two ellipsoids. In order to describe the relative position and orientation between one ellipsoid and one sphere, the Euler angles φ and θ are not necessary when the ellipsoid E_1 is fixed at the origin of the X-Y-Z coordinate system and axis of revolution is in line with the Y-axis, as shown in Fig. 3. In this case, only three parameters (α, β and r) are required to describe the relative position of two particles.

Look-up tables are generated for the ellipsoid-ellipsoid and ellipsoid-sphere interactions, respectively. The range of parameters is listed in Table I. Only positive values for the parameter range are listed here, since for combinations of parameters that include negative values an equivalent positive parameter combination can always be found using symmetry. The symbol a denotes the length of the long semi-axis of the AM ellipsoid, a_{CB} is the radius of CB particles, and r_0 is the distance of closest approach between two particles at a given combination of α, β, φ and θ. The distance of closest approach is the distance between the centers of the particles when they are exter-

Table I. Look-up table parameter range for (a) ellipsoid-ellipsoid and (b) ellipsoid-sphere interactions.

(a)	Parameter	Range	Number of intervals and increment
	r	$1.01r_0 \sim 5a$	20 intervals, logarithmical scale
	α	$0 \sim \pi/2$	15 intervals with an increment of $\pi/30$
	β	$0 \sim \pi/2$	15 intervals with an increment of $\pi/30$
	ϕ	$0 \sim \pi/2$	15 intervals with an increment of $\pi/30$
	θ	$0 \sim \pi/2$	15 intervals with an increment of $\pi/30$
(b)	Parameter	Range	Number of intervals and increment
	r	$1.01r_0 \sim 1.8(a+a_{CB})$	20 intervals, logarithmical scale
	α	$0 \sim \pi/2$	64 intervals with an increment of $\pi/128$
	β	$0 \sim \pi/2$	64 intervals with an increment of $\pi/128$

Table II. (a) Material properties associated with the electrode materials (b) Design of experiment.

(a)	Material	Density (g/cm^3)	Hamaker constant (J)	Dielectric constant		
	CB	2.0	2.53×10^{-19}	-		
	MnOx	4.0	1.59×10^{-18}	-		
	NMP	-	8.21×10^{-20}	32.2		
(b)	Mass ratio (CB:AM)	AM aspect ratio (a/b)	CB diameter (μm)	AM semi-axes (μm)	Number of CB particles	Number of AM particles
	2% : 94%	2	0.06	a = 0.3969 b = c = 0.1984	616	20
		3	0.06	a = 0.5200 b = c = 0.1733	616	20
	4% : 92%	2	0.06	a = 0.3969 b = c = 0.1984	1258	20
		3	0.06	a = 0.5200 b = c = 0.1733	1258	20

nally tangent; it is calculated with the algorithm developed by Zheng et. al.[27,28]

The interaction potential ΔG_{12}^{d} is calculated according to Eq. 16 through a numerical integration using Mathematica 7 and tabulated in the five-dimensional parameter space for ellipsoid-ellipsoid interactions or three-dimensional parameter space for ellipsoid-sphere interactions. During the Monte Carlo simulation, the interaction potential is calculated for a given combination of relative position and relative orientation through interpolation, using 5 closest data points in each dimension of the parameter space. At center-to-center distances shorter than the cutoff distance (1.01 r_0 for AM-AM and AM-CB interaction, 1.001 r_0 for CB-CB interaction), the potential is replaced by a cutoff potential in order to avoid divergence in the interaction energy.

Simulation parameters.— The formation of composite electrodes is modeled. The electrode structures are: mixtures of manganese oxide as the active material, carbon black as the conductive additive, and PVDF as the polymeric binder. AM particles are simulated as prolate spheroids with an aspect ratio of 2 or 3. The volume of an ellipsoid is equal to that of a 0.5 μm diameter sphere. CB particles are simulated as spheres with a diameter of 60 nm, assuming that they start from a very low level of agglomeration prior to the mixing process. PVDF binder is dissolved in an Anhydrous *N*-methylpyrrolidone (NMP) solution, forming a homogenous viscous medium. The material properties of the constituents of the electrode structure can be found in Table II.[7]

Two different mass ratios are considered, where CB:AM:PVDF is 2% : 94% : 4% or 4% : 92% : 4%. The volume fraction of the total solid phase (CB, AM, PVDF, after the NMP solvent evaporates) in the simulation domain is 50%. In this work, 20 AM particles are added inside the domain with periodic boundary conditions. The size of the simulation domain and the number of CB particles are calculated from the solid volume fraction and mass ratio of CB:AM. The number of CB particles is 1,258 for a CB:AM ratio of 4%:92% and 616 for a CB:AM ratio of 2%:94%. The temperature is fixed at 298 K.

Aggregated structure characterization.— The final aggregates obtained from the Monte Carlo simulations were characterized in terms of the amount of CB connected to the AM cluster. During the simulations, it is recorded whether each pair of particles was connected. Using this information, we built a cluster list in which the connected particles were grouped in the same cluster. The connection between CB particles and AM particle clusters is an important parameter, since only when conductive additives connect with active material do they contribute to the overall conductivity of the system. At a given CB content, it is reasonable to assume that the more CB particles are connected to AM particle clusters, the bigger contribution they make toward improving the conductivity of the cathode system. Therefore, we characterize the aggregated system by the percentage of CB particles connected to the AM particles, using the cluster list we found.

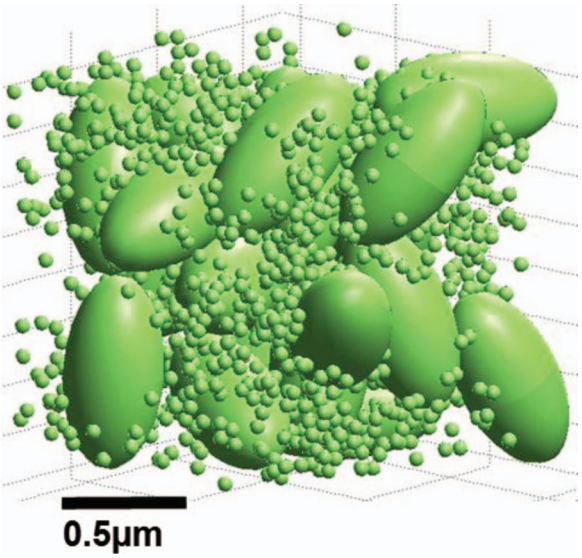

Figure 4. Representations of the final stabilized configuration for aggregates with ellipsoidal active material particles and spherical conductive additive particles (AM aspect ratio = 2, CB : AM mass ratio = 4% : 92%).

Results and Discussion

We conducted 5 Monte Carlo simulation cases for each parameter combination shown in Table II(b). Figure 4 shows a representation of the final stabilized configuration of the system containing ellipsoidal active material particles. The larger ellipsoids represent AM particles while the smaller spheres represent CB particles. In all cases, AM particles form a percolated network. The CB particles are connected to AM particles and also form local clusters among themselves. Some of these clusters are attracted to the AM particle network, contributing to the conductivity of the electrode. The resulting aggregated structures are characterized, and the percentage of CB particles connected to the clusters of ellipsoidal AM particles for each parameter combination is plotted in Fig. 5. If the mass ratios of CB and AM are kept the same, the average percentage of CB particles attached to the ellipsoid AM

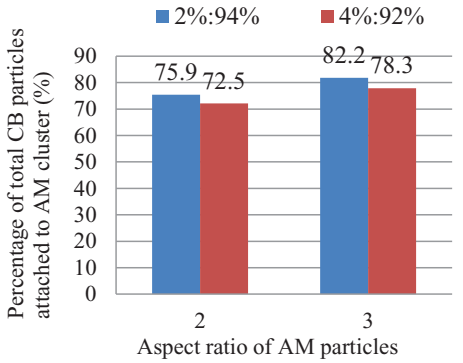

Figure 5. Number of CB connected to AM cluster for different AM particle aspect ratios and CB : AM mass ratios.

Table III. Cathode optimization for specific energy and conductivity.

AM aspect ratio (a/b)	1			2		3	
Mass ratio (CB:AM)	4% : 92%		8% : 88%	2% : 94%	4% : 92%	2% : 94%	4% : 92%
AM size (spherical diameter)	1.0 μm			0.5 μm*			
Specific energy (Ah/kg)	129	129	123	132	129	132	129
Mass of attached CB (% of total cathode mass)	1.73%	1.05%	7.25%	1.52%	2.90%	1.64%	3.13%

*For ellipsoidal AM particles, the particle volume equals to that of a sphere with a diameter of 0.5 μm.

particle cluster is found to be higher as the aspect ratio increases from 2 to 3. For cases where the AM particle aspect ratio is kept the same, the average percentage of CB attachment is decreased as the CB:AM mass ratio increases from 2%:94% to 4%:92%.

The simulation results show that a larger aspect ratio contributes positively to the CB particles attachment rate. If we include the comparable results of our previous work[7] about spherical particles, it is shown that when particle aspect ratio increases from 1 to 3, the CB attachment rate increases from 26.3% to 78.3% (for a CB:AM mass ratio of 4%:92%) as shown in Fig. 6. For active material particles of the same volume, the surface area increases with the aspect ratio, promoting CB attachment.

The mass ratio of CB:AM contributes negatively to the CB attachment rate within the simulation parameters used in this work (CB:AM = 2%:94% and 4%:92%). However, in our previous spherical particle work, the CB attachment rate increases with increasing CB:AM mass ratio (CB:AM = 4%:92% and 8%:88%). One possible explanation is as follows: for cases where CB concentration is very low (2%:94%), a higher percentage of CB are attracted to the larger AM particles. When the CB concentration is higher (4%:92%), the CB particles tend to self-aggregate, forming their own colonies and thus hindering the attachment to AM particles. However, when the CB concentration further increases (8%:88%), the effect of "percolation" starts to become dominant. Therefore, although CB particles still tend to aggregate with themselves, the possibility of connection pathways formed between these CB colonies and AM particles increases with the increased number of CB particles.

It also needs to be noted that the percentage of CB attachment (CB utilization) doesn't necessarily translate to higher electrical conductivity in real world cathodes. In the case of CB:AM = 2%:94%, although a high percentage of CB particles are attached to AM particle surface, the conductive pathways may be fewer than other cases due to the fewer numbers of particles.

When it comes to optimization of Li-ion batteries, conductivity and specific energy need to be considered. Since the total mass of the carbon black particles that attach to the active material and form conductive paths is directly related to the conductivity of the cathode, we calculated this mass as a fraction of the total mass of the cathode system and listed the values for each parameter combination in Table III. The specific energy of the cathode system (containing AM, CB and PVDF) for each case was also calculated, assuming that the theoretical capacity for $Li_xMn_2O_4$ is 140Ah/kg.

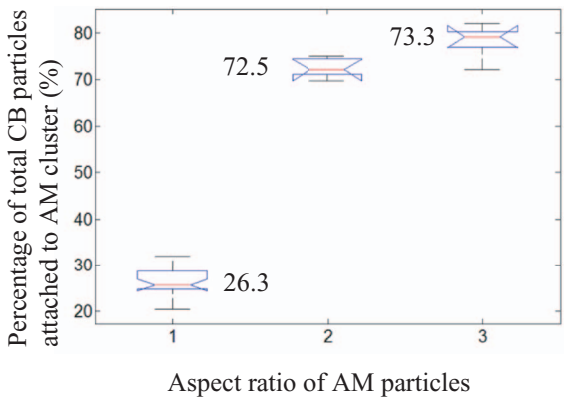

Figure 6. Number of CB connected to AM cluster for AM particles with different aspect ratios.

Table III shows that conductivity is most sensitive to the additive-active material mass ratio. In the cases of AM aspect ratio = 1, when the conductive additive mass is increased from 4% to 8% of the total cathode mass, the total mass of attached CB increases from below 2% to 7.25% of the total cathode mass. In the cases of AM aspect ratio = 2 and 3, although the percentage of CB attached to AM particle slightly decreases, the total mass of attached CB increases significantly. At the same time, the specific energy decreases by less than 5%. This decrease of specific energy can be justified by the significantly increased conductivity. Larger active material particle size and aspect ratio are also preferable as long as the particle size is kept under 1.0 μm, ensuring that fracture will be unlikely for discharge rates under 10 C.[6]

In future work, a link between CB - AM connection morphology and actual cathode conductivity needs to be established so that optimization can be performed to improve battery performance.

The Monte Carlo method was used in this work instead of Brownian dynamics, which was used in the case of spherical particles.[7] Capable of sampling energetically favorable configurations and extracting the information we are interested in, the Monte Carlo method does not require the implementation of collision and momentum transfer between particles which involves complicated rigid body motion and interaction of ellipsoids (linear translation and rotation), thus drastically reducing the computational cost compared to Brownian dynamics for ellipsoidal particles. However, the Brownian dynamics simulation handles the collective motion of particles better than Monte Carlo, since the latter only allows one particle to move at a time.

The implementation of a look-up table provides an accurate and efficient method of finding interaction energy for a generalized ellipsoid system, compared with the computationally intensive direct integration method and the approximation method, both of which have only a narrow applicable range. The accuracy of this method can be further enhanced by increasing the resolution of the look-up table. This method also has a benefit of being readily extendable to different types of interaction potentials other than the pair-wise additive inverse power law potential discussed in this work. The limitation of this look-up table is that for each new aspect ratio a new look-up table needs to be generated. For a system containing N types of particles (different particle type means different material, aspect ratio and/or different size), a total of N! look-up tables need to be generated in advance. This may not be practical to implement in systems containing particles with continuously varying shapes and sizes.

In this work, the electrostatic double layer interaction potential is not considered. Van der Waals interaction is shown in the previous work to be dominant so that the electrostatic double layer contribution can be omitted.[7]

Conclusions

It is known that the aggregation of inactive and active materials in Li-ion battery electrodes greatly impact the conductivity and power performance of the electrodes. This work extends our previous effort[7] by including non-spherical particles and exploring various CB:AM mass ratios. These two works are the first attempt to numerically

simulate the aggregation process in Li-ion battery electrodes with Brownian dynamics and Monte Carlo methods to reveal the effects of particle shape, size and mass ratio on the packing of cathode particles. From a wide range of numerical experiments, it is found that the particle geometry including size and aspect ratio plays an important role in determining the internal particle network. The connectivity of the active particles and additive particles is critically important for obtaining sufficient conductivity to transfer electronics. However, the additive material does not store energy, so finding the optimal ratio of this additive material is necessary to maximize the energy density of a Li-ion battery. This work may provide a tool for guiding the optimization of electrode materials.

Acknowledgments

This research was funded by the GM /UM Advanced Battery Coalition for Drivetrains. Support from our sponsor is gratefully acknowledged.

References

1. D. H. Jang, Y. J. Shin, and S. M. Oh, *J. Electrochem. Soc.*, **143**, 2204 (1996).
2. D. H. Jang and S. M. Oh, *J. Electrochem. Soc.*, **144**, 3342 (1997).
3. J. Park, J.-H. Seo, G. Plett, W. Lu, and A. M. Sastry, *Electrochem. Solid-State Lett.*, **14**, A14 (2011).
4. G. Liu, H. Zheng, X. Song, and V. S. Battaglia, *J. Electrochem. Soc.*, **159**, A214 (2012).
5. J. Park, S. Kalnaus, S. Han, Y.-K. Lee, G. B. Less, N. J. Dudney, C. Daniel, and A. M. Sastry, *J. Power Sources*, **222**, 417 (2013).
6. M. Zhu, J. Park, and A. M. Sastry, *J. Electrochem. Soc.*, **159**, A492 (2012).
7. M. Zhu, J. Park, and A. M. Sastry, *J. Electrochem. Soc.*, **158**, A1155 (2011).
8. H. Wang, Y.-I. Jang, B. Huang, D. R. Sadoway, and Y.-M. Chiang, *J. Electrochem. Soc.*, **146**, 473 (1999).
9. M.-R. Lim, W.-I. Cho, and K.-B. Kim, *J. Power Sources*, **92**, 168 (2001).
10. D. Wang, X. Wu, Z. Wang, and L. Chen, *J. Power Sources*, **140**, 125 (2005).
11. S. Zeng, K. Tang, T. Li, Z. Liang, D. Wang, Y. Wang, Y. Qi, and W. Zhou, *J. Phys. Chem. C*, **112**, 4836 (2008).
12. J. Liu, H. Xia, L. Lu, and D. Xue, *J. Mater. Chem.*, **20**, 1506 (2010).
13. V. Agubra and J. Fergus, *Materials*, **6**, 1310 (2013).
14. J. Park, W. Lu, and A. M. Sastry, *J. Electrochem. Soc.*, **158**, A201 (2011).
15. S. Ross and I. D. Morrison, *Colloidal Systems and Interfaces*, John Wiley & Sons, New York (1988).
16. S. N. Fejer, D. Chakrabartia, and D. J. Wales, *Soft Matter*, **7**, 3553 (2011).
17. G. Veble and R. Podgornik, *Eur. Phys. J. E*, **23**, 275 (2007).
18. R. Golestanian, *Phys. Rev. Lett.*, **95**, 230601 (2005).
19. M. S. Oversteegen and H. N. W. Lekkerkerker, *Phys. Rev. E*, **68**, 021404 (2003).
20. S. Kruger, H.-J. Mogel, M. Wahab, and P. Schiller, *Langmuir*, **27**, 646 (2011).
21. P. Schiller, S. Kruger, M. Wahab, and H.-J. Mogel, *Langmuir*, **27**, 10429 (2011).
22. J. Moscinski, M. Bargiel, Z. A. Rycerz, and P. W. M. Jacobs, *Mol. Simul.*, **3**, 201 (1989).
23. B. D. Lubaehevsky and F. H. Stillinger, *J. Stat. Phys.*, **60**, 561 (1990).
24. A. Donev, F. H. Stillinger, P. M. Chaikin, and S. Torquato, *Phys. Rev. Lett.*, **92**, 255506 (2004).
25. Y.-B. Yi and A. M. Sastry, *Proc. R. Soc. Lond. A*, **460**, 2353 (2004).
26. J. Vieillard-Baron, *J. Chem. Phys.*, **56**, 4729 (1972).
27. X. Zheng and P. Palffy-Muhoray, *Phys. Rev. E*, **75**, 061709 (2007).
28. X. Zheng, W. Iglesias, and P. Palffy-Muhoray, *Phys. Rev. E*, **79**, 057702 (2009).